minerals

MDPI

Article

Predicting the Release and Migration of Potentially Harmful Elements (PHEs) during the Lightweight Ceramsite Preparation from Carbide Slag

Qi Jiang [1], Yongmei He [1], Yonglin Wu [1], Tianguo Li [1], Chengxue Li [1], Hongpan Liu [2], Zhonghua Wang [3] and Ming Jiang [1,*]

[1] College of Resources and Environment, Yunnan Agricultural University, Kunming 650201, China
[2] College of Materials and Chemical Engineering, Chongqing University of Arts and Sciences, Chongqing 402160, China
[3] Faculty of Environmental Science and Engineering, Kunming University of Science and Technology, Kunming 650500, China
* Correspondence: mingjiang2010@163.com

Abstract: When preparing lightweight ceramsite using carbide slag, trace amounts of toxic elements are released into the atmosphere due to high-temperature calcination, posing a significant risk to the environment. The real-time monitoring of the released gases is challenging under laboratory conditions while preparing large quantities of ceramsite. Therefore, heating was simulated using experimental data and the FactSage 7.0 thermochemical database to study the release of harmful Al-, C-, H-, S-, and F-containing elements when using carbide slag to prepare lightweight ceramsite. The results indicated that no Al, C, H, S, or F elements were evident in the high-temperature liquid products obtained in a 50 °C to 1150 °C calcination temperature range. Al was present in a solid state with no gaseous products. When the temperature reached 450 °C, CO gas was released and its level increased as the temperature rose. H and S mainly combined into H_2S gas, starting at 250 °C and reaching a peak at 1050 °C. H and F primarily combined into HF, starting at 400 °C. Other F-containing gases mainly included SiF_4 and TiF_3, which began to release at 800 °C and 900 °C, respectively. The release trends of HF, SiF_4, and TiF_3 were consistent with those of CO. This study aimed to conduct an environmental impact and management assessment for the preparation of lightweight ceramsite using carbide slag. The use of raw material carbide slag for the low-cost treatment of tail gas was proposed, which provides theoretical and up-to-date support for greening the application of the process.

Keywords: carbide slag; lightweight ceramsite; FactSage; gaseous contaminants

check for updates

Citation: Jiang, Q.; He, Y.; Wu, Y.; Li, T.; Li, C.; Liu, H.; Wang, Z.; Jiang, M. Predicting the Release and Migration of Potentially Harmful Elements (PHEs) during the Lightweight Ceramsite Preparation from Carbide Slag. *Minerals* **2023**, *13*, 216. https://doi.org/10.3390/min13020216

Academic Editors: Anna Bogush, Tongsheng Zhang and Elena Khayrulina

Received: 27 December 2022
Revised: 29 January 2023
Accepted: 31 January 2023
Published: 2 February 2023

1. Introduction

Polyvinyl chloride (PVC) is primarily produced via calcium carbide smelting in China. When calcium carbide is hydrolyzed to acetylene, many calcium-containing byproducts are produced as carbide slag, with $Ca(OH)_2$ as the main component [1,2]. Manufacturing 1 ton of PVC produces about 1.5 tons of carbide slag [3], occupying land resources while causing water pollution and other problems [4]. A previous study indicated that heavy metals in carbide slag, such as Pb and Sr, pose potential ecological risks [5]. Resource utilization is essential to reducing the hazardous nature of solid waste. This can be achieved by recycling the expanded polystyrene waste to remove the phenol from water [6], using sago waste or waste fish bones to remove the heavy metals from water, and so on [7,8]. Therefore, reutilization methods have been proposed to prepare $CaSO_4$, $CaCO_3$ [9,10], CaO briquettes [11], aerated concrete [12], and adsorption materials [13] for the alleviation of the environmental threat from carbide slag. Currently, the resource utilization of carbide slag is still focused on the production of building materials.

Lightweight ceramsite is an important building material and environmental protection material. It can be produced using carbide slag as the raw material [14–18]. However, high-temperature calcination is essential for preparing ceramsite. Consequently, the harmful components in carbide slag migrate and transform with an increase in calcination temperature. Parts of the components are released into the air. Gaseous pollutants that are easy to disperse and difficult to treat can affect ambient air quality and human health when a large amount of carbide slag is used to produce lightweight ceramsite. Therefore, the potential environmental risks of using industrial solid waste to produce building materials have gained great attention. Predicting the release and migration of trace hazardous components in raw materials during calcination and effectively controlling the resulting contaminants has become a challenge.

FactSage [19] is a software for chemical thermodynamic calculation. It is used for simulations in many fields, such as material science, metallurgy, the chemical industry, environmental science, and combustion science [20]. Studies that cannot be conducted under specific experimental conditions (e.g., high temperature, high pressure, etc.) can be carried out via the prediction and simulation of the data using FactSage. In addition, FactSage can calculate multiphase equilibrium conditions for a wide range of constraints. For example, the effect of concentration and temperature on the leaching of fluorescent lamp powder with sulfuric acid was evaluated by FactSage [21]. The software was also used to explore the effect of additives on sludge and fouling during Zhundong coal gasification [22]. FactSage was also used to calculate the linear relationship between the melting behavior and temperature of ash [23], determine the best operating parameters of a blast furnace [24], and predict the ash melting behavior in reducing conditions [25]. However, the prediction of the migration behavior of hazardous components produced during the preparation of lightweight ceramsite using carbide slag has not been reported.

The raw materials used in producing ceramsite from carbide slag contain various chemical components. Of these, Al can damage the human central nervous system, while C, H, S, and F are rapidly released when influenced by temperature. Therefore, further research into these five elements is required. This study qualitatively and quantitatively analyzed carbide slag samples, and, combined with the proportion of the ceramsite raw materials described in ref. [18], predicted the release and migration characteristics of Al, C, H, S, and F during raw material calcination (50–1150 °C) using FactSage 7.0. Prevention and control methods to restrict gaseous pollutant release and render this process more environmentally friendly are proposed.

2. Materials and Methods

2.1. Pretreatment of Materials

The following procedure was used to pretreat the materials:

Grinding: Carbide slag (Anning, Yunnan, China) was ground in a planetary ball mill (YXQM, Changsha MITR Instrumentation Co., Ltd., Changsha, China).

Drying: The ground carbide slag was dried in a vacuum drying oven (DZF-6090, Shanghai JINYOU test equipment Co., Ltd., China) at 100 °C for 24 h.

Sieving: The dried carbide slag was passed through a 180-mesh sieve (85 μm opening).

2.2. Analytical Methods

Since X-ray fluorescence (XRF) spectrometry (ZSX-100e, Rigaku, Tokyo, Japan) could not determine if the H elements and the quantification of C and N elements were inaccurate, an organic elemental analyzer (VarioEL III, Elementar, Langenselbold, Germany) was used to initially determine the C, H, and N elements. The test conditions included the use of the dynamic combustion method, an oxidation furnace temperature of 950 °C, and a reduction furnace temperature of 850 °C. The remaining elements were determined via XRF. The test conditions included an Rh target, a voltage of 50 kV, and a 60-mA current. The test results are shown in Table 1.

Table 1. Chemical composition of carbide slag (wt%).

Composition	SiO_2	Al_2O_3	CaO	Fe_2O_3	TiO_2	MgO	Na_2O	C	H	S	F
Content	5.67	4.63	75.03	3.34	0.87	0.31	0.13	6.81	2.17	0.53	0.35

2.3. Raw Material Formulas and Analysis

The formulas used for the ceramsite raw materials are described in ref. [18]. The specific content of each component is listed in Table 2. There, mainly included is SiO_2, Al_2O_3, and CaO. Therefore, to prepare the SiO_2-Al_2O_3-CaO ternary ceramsite, the three components were normalized while the content of the other components remained unchanged. After normalization, the SiO_2, Al_2O_3, and CaO levels were 60.78 wt%, 20.54 wt%, and 18.68 wt%, respectively. This is considered to be the basic formula for the SiO_2–Al_2O_3–CaO ternary ceramsite.

Table 2. Primary composition of raw materials of lightweight ceramsite (wt%).

Raw Material Composition	SiO_2	Al_2O_3	CaO	Fe_2O_3	K_2O	Na_2O	MgO	Other
Tail mud	61.69	20.83	3.58	3.71	3.14	1.64	0.79	2.80
Carbide slag	2.95	1.07	62.45	0.84	-	-	0.23	21.33
Total	49.94	16.88	15.35	3.14	2.51	0.31	0.68	6.51

Note: tail mud: carbide slag = 4:1, mass ratio.

Although the carbide slag displayed a high CaO content (Table 1), minimal levels were evident in the raw ceramsite materials (Table 2). Therefore, the SiO_2-Al_2O_3-CaO ternary ceramsite was obtained by adding an appropriate amount of Al_2O_3 and SiO_2 to the carbide slag, which was calculated based on the CaO content. The total component mass of the carbide slag-based ceramsite was 75.03 g/18.68 wt% = 401.66 g. When using 100 g of carbide slag, the mass of the SiO_2, Al_2O_3, and CaO in the SiO_2-Al_2O_3-CaO ternary ceramsite was 244.13 g, 82.50 g, and 75.03 g, respectively, while that of the SiO_2 and Al_2O_3 added to the carbide slag was 238.46 g and 77.87 g, respectively. The proportion of ceramsite raw materials was calculated (Table 3). The Al, C, H, S, and F composition and distribution at thermodynamic equilibrium were calculated during raw material calcination and heating using the Equilib phase calculation module, oxide database (FToxid-SlagH), and Fact Pure Substances database (FactPs) of the FactSage 7.0 software. Before simulation, the hypothesis and calculation parameters were set as follows: (1) The gas-phase equilibrium products generated during the reaction were considered ideal gases and the high-temperature molten-phase products generated were considered liquid-phase products. (2) The input reactant was calculated according to the chemical composition of the ceramsite raw materials listed in Table 3, and the input was expressed in grams. (3) The reaction pressure was 1.01×10^5 Pa, while the temperature was maintained in a range of 50 °C to 1150 °C at 50 °C increments.

Table 3. The composition of the SiO_2-Al_2O_3-CaO lightweight ceramsite.

Composition	SiO_2	Al_2O_3	CaO	Fe_2O_3	TiO_2	MgO	Na_2O	C	H	S	F
Carbide slag/g	5.67	4.63	75.03	3.34	0.87	0.31	0.13	6.81	2.17	0.53	0.35
Additive (SiO_2/Al_2O_3)/g	238.46	77.87	0								
Composite/g	244.13	82.50	75.03	3.34	0.87	0.31	0.13	6.81	2.17	0.53	0.35

3. Results and Discussion

3.1. Equilibrium Product Production of Each Phase

The FactSage calculation results showed that no liquid-phase products containing Al, C, H, S, or F were formed during the calcination and heating of the ceramsite raw materials. Figure 1 shows the variation trend in the gas-phase and solid-phase equilibrium products

comprising Al, C, H, S, or F based on temperature, which did not change significantly upon increasing the temperature. Over the whole temperature range, only the solid-phase conversion of Al elements occurred, and no gas-phase products were generated; the generation of gas-phase equilibrium products comprising S and F was very low. When the temperature exceeded 1000 °C, the amount of F-containing gaseous pollutants increased slightly, but the S-containing gaseous pollutants decreased gradually, indicating that the high-temperature stage (>1000 °C) accelerated the volatilization of F in the ceramsite raw materials. However, the amount of C-containing gas-phase equilibrium products decreased gradually upon increasing the temperature, and the amount of corresponding solid-phase equilibrium products increased gradually upon increasing the temperature. This might be due to the gradual transformation of some C-containing gas-phase products into solid-phase products during the heating process.

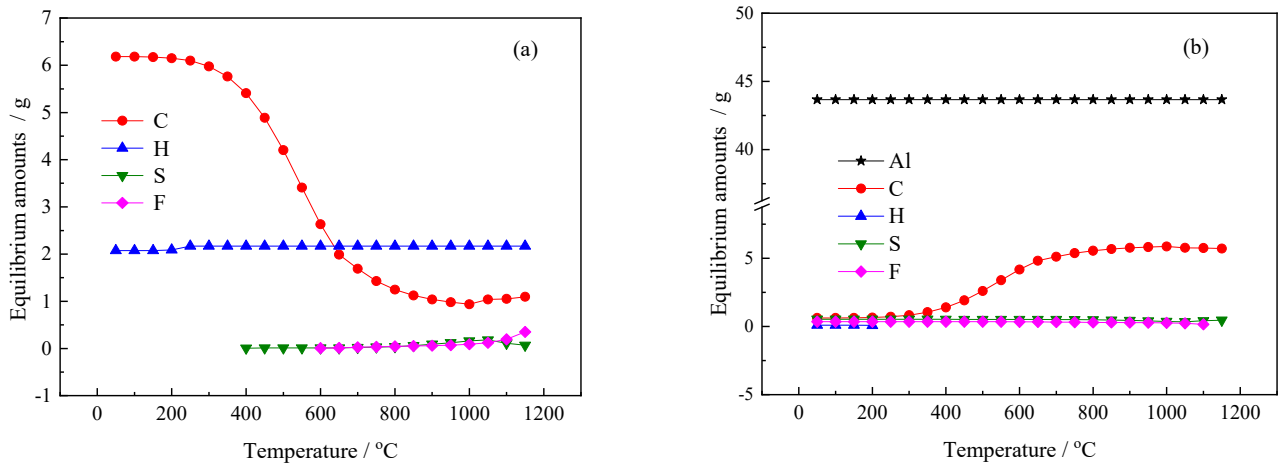

Figure 1. Equilibrium amounts of products in gas phase (**a**) and solid phase (**b**).

3.2. Migration and Transformation of Aluminum

Figure 2 shows the distribution of Al in each phase during the firing of ceramsite. Al always existed in the solid phase during heating and calcination, and no Al-containing gas-phase product was found. Among them, $Fe_3Al_2Si_3O_{12}$ (almandite) existed only at 50 °C. $Ca_2Al_3Si_3O_{12}(OH)$ (zoisite) and $Ca_3Al_2Si_3O_{12}$ (grossularite) disappeared at 250 °C and 450 °C, respectively. During the initial temperature increase stage (50–600 °C), the $CaAl_2Si_2O_8$ (anorthite) content increased with an increase in temperature. When the temperature exceeded 650 °C, a small amount of $CaAl_2Si_2O_8$ (0.26 wt%) was transformed into $NaAlSi_3O_8$ (albite).

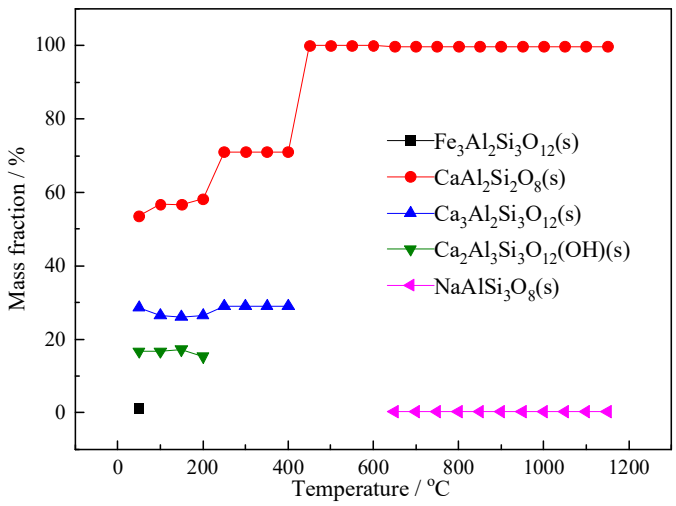

Figure 2. Distribution of aluminum products in different phases during the heating process.

3.3. Migration and Transformation of Carbon

Figure 3 shows the forms of C in each phase of ceramsite during heating. Gaseous substances included CH_4, CO_2, and CO. The mass fractions of C and H_2 (Figure 4) increased with the temperature, which showed that the migration and transformation of CH_4 mainly occurred due to the cracking of methane [26] (Equation (1)).

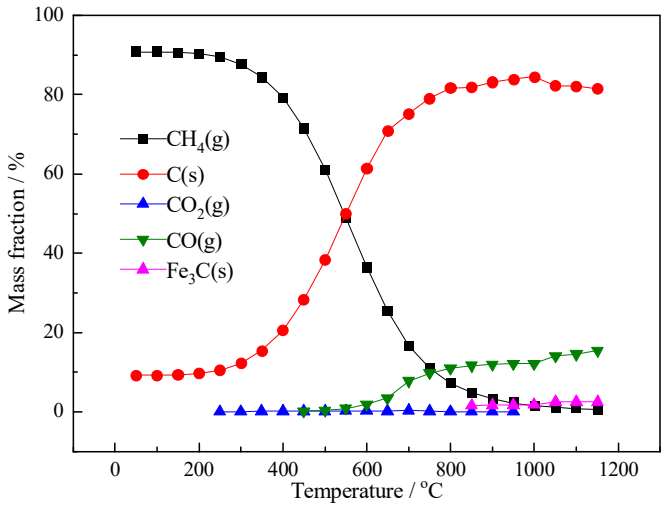

Figure 3. Distribution of carbon products in different phases during the heating process.

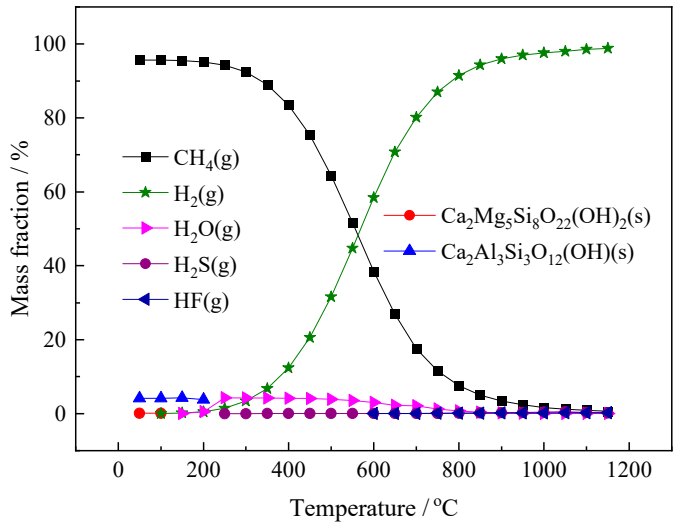

Figure 4. Distribution of hydrogen products in different phases during the heating process.

When the calcination temperature reached 250 °C, gaseous CO_2 began to appear in the reaction system, and its release decreased with an increase in temperature. It peaked to 0.34 wt% at 700 °C and completely disappeared at 950 °C, indicating that CO_2 was an intermediate product. This was because a small amount of O_2 reacted with the solid-phase C to produce CO_2 first, which was then reduced to the gas-phase CO by C (Equations (2) and (3)). When the calcination temperature reached 450 °C, CO began to appear, and its release increased gradually with an increase in temperature. When the maximum calcination temperature was 1150 °C, the mass fraction of CO reached 15.42 wt%. This was because when the temperature was higher than 450 °C, the main substance $Ca(OH)_2$ in carbide slag began to decompose, and the water–gas reaction between C and the decomposition product to the gas-phase H_2O led to the increased CO release (Equations (4) and (5)).

When the calcination temperature reached 850 °C, the solid Fe_3C (cementite) began to appear, whose mass fraction increased with an increase in temperature and remained

unchanged after reaching the peak of 2.46 wt% at 1050 °C. Fe_3C was formed due to the solid-state reaction between Fe_2O_3 and C in carbide slag [27,28]. This reaction occurred because of an increase in the gas-phase CO release (Equations (6) and (7)).

$$CH_4(g) \rightarrow C(s) + 2H_2(g) \quad (1)$$

$$C(s) + O_2(g) \rightarrow CO_2(g) \quad (2)$$

$$CO_2(g) + C(s) \rightarrow 2CO(g) \quad (3)$$

$$Ca(OH)_2(s) \rightarrow CaO(s) + H_2O(g) \quad (4)$$

$$C(s) + H_2O(g) \rightarrow CO(g) + H_2(g) \quad (5)$$

$$3C(s) + Fe_2O_3(s) \rightarrow 2Fe(s) + 3CO(g) \quad (6)$$

$$C(s) + 3Fe(s) \rightarrow Fe_3C(s) \quad (7)$$

3.4. Migration and Transformation of Hydrogen

Figure 4 shows the distribution of H in each phase during the firing of ceramsite. Gaseous H-containing products included CH_4, H_2, H_2O, H_2S, and HF. Solid substances, which include $Ca_2Mg_5Si_8O_{22}(OH)_2$ (tremolite) and $Ca_2Al_3Si_3O_{12}(OH)$ (tanzanite), only formed at calcination temperatures below 200 °C, and their mass fractions remained unchanged. When the calcination temperature gradually increased, $Ca_2Mg_5Si_8O_{22}(OH)_2$ and $Ca_2Al_3Si_3O_{12}(OH)$ decomposed. The existence of CH_4, H_2, and H_2O was discussed in the previous section.

H_2S gas was generated when the calcination temperature reached 250 °C and its release peaked at 1050 °C. Combined with the changes discussed in the mass fractions of FeS and H_2S in the previous section, it was hypothesized that H_2S was formed by the reaction of FeS with H_2 and H_2O, respectively [29,30] (Equations (8) and (9)). When the calcination temperature reached 600 °C, HF gas was generated and HF release increased with an increase in calcination temperature. Combined with the changes in the mass fractions of CaF_2, HF, and SiF_4 discussed in the previous section, it was hypothesized that CaF_2 reacted with SiO_2 in ceramsite raw materials to form SiF_4 [31], which was further hydrolyzed to form H_4SiO_4 and HF (Equations (10) and (11)). The highly unstable solid-phase H_4SiO_4 then decomposed into SiO_2 and H_2O (Equation (12)). H_2S and HF are the gas-phase substances that need to be focused on in the actual production process due to their severe toxicity characteristics.

$$FeS(s) + H_2(g) \rightarrow H_2S(g) + Fe(s) \quad (8)$$

$$FeS(s) + H_2O(g) \rightarrow H_2S(g) + FeO(s) \quad (9)$$

$$7SiO_2(s) + 6CaF_2(s) \rightarrow 2Ca_3Si_2O_7(s) + 3SiF_4(g) \quad (10)$$

$$SiF_4(g) + 4H_2O(g) \rightarrow H_4SiO_4(s) + 4HF(g) \quad (11)$$

$$H_4SiO_4(s) \rightarrow SiO_2(s) + 2H_2O(g) \quad (12)$$

3.5. Migration and Transformation of Sulfur

Figure 5 shows the distribution of S in each phase during the firing of ceramsite. When the temperature was in the range of 50–750 °C, only solid-phase FeS and gas-phase H_2S existed in the system. The migration and transformation trends of FeS and H_2S were consistent with the results discussed in the previous section.

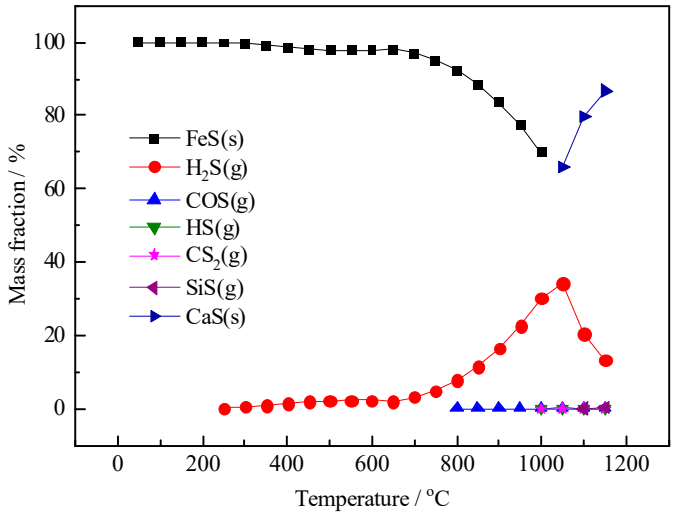

Figure 5. Distribution of sulfur products in different phases during the heating process.

The gaseous-phases of COS, HS, CS_2, and SiS were generated in the high-temperature stage of calcination, and their release was at a low level (<0.1 wt%). As depicted in Equations (13)–(16), it was hypothesized that COS was released due to the reaction of H_2S with the CO_2 (Equation (2)), and that CS_2 was generated due to the decomposition of COS and the reaction of H_2S with CO_2 and COS [32,33]. Moreover, HS in this reaction system might have been formed due to an intermediate that was generated by the gas-phase reaction between H_2S and O_2 [34] (Equation (17)). HS radicals might not have a serious impact on the atmospheric environment due to their instability.

When the calcination temperature reached 1050 °C, solid CaS with a mass fraction of 65.68 wt% appeared, which increased to 86.8 wt% with an increase in temperature. It was hypothesized that in the middle of the heating stage (400–800 °C), the high-temperature calcination solid-phase product of carbide slag, CaO, was formed, and CaS, which was the product of the reaction between H_2S and CaO, was hydrolyzed [35]. This hypothesis could reasonably explain why CaS was not produced in the middle of the heating period, besides the lower release of H_2O and higher release of H_2S (Figure 4). When the calcination temperature reached 1050 °C, FeS was replaced by Ca and formed solid-phase CaS. H_2O in the system was consumed, and the hydrolysis reaction of CaS no longer occurred. Meanwhile, H_2S continued to react with CaO to form CaS. Therefore, the release of H_2S decreased, and the content of CaS increased above 1050 °C. The expected series of reactions is described by Equations (4) and (18)–(20).

Gaseous SiS began to be released at 1100°C, and its release increased with an increase in the calcination temperature. It was hypothesized that it was generated by the reaction between C, produced by the cracking of CaS, CH_4, and SiO_2 in the raw material [36]. This result explained the higher release of CO in the later heating phase (Equation (21)).

$$H_2S(g) + CO_2(g) \rightarrow COS(g) + H_2O(g) \quad (13)$$

$$2COS(g) \rightarrow CS_2(g) + CO_2(g) \quad (14)$$

$$H_2S(g) + COS(g) \rightarrow CS_2(g) + H_2O(g) \quad (15)$$

$$2H_2S(g) + CO_2(g) \rightarrow CS_2(g) + 2H_2O(g) \quad (16)$$

$$H_2S(g) + O_2(g) \rightarrow HS(g) + HO_2(g) \quad (17)$$

$$CaS(s) + 2H_2O(g) \rightarrow H_2S(g) + Ca(OH)_2(s) \quad (18)$$

$$FeS(s) + CaO(s) \rightarrow CaS(s) + FeO(s) \quad (19)$$

$$H_2S(g) + CaO(s) \rightarrow CaS(s) + H_2O(g) \quad (20)$$

$$CaS(s) + C(s) + SiO_2(s) \rightarrow SiS(g) + CaO(s) + CO(g) \quad (21)$$

3.6. Migration and Transformation of Fluorine

Figure 6 shows the distribution of F in each phase during the firing of ceramsite. F existed only in the form of solid CaF_2 in the initial heating stage (<350 °C), and its mass fraction decreased with an increase in the calcination temperature, until it disappeared at 1100 °C. In this system, the gaseous-phases HF and SiF_4 began to be released at 400 °C and 800 °C, respectively, and the released amounts increased with an increase in the calcination temperature. The maximum released amounts were 29.94 wt% and 24.88 wt%, respectively. The migration and transformation trends of CaF_2, HF, and SiF_4 were consistent with the results discussed in the Migration and Transformation of Hydrogen section.

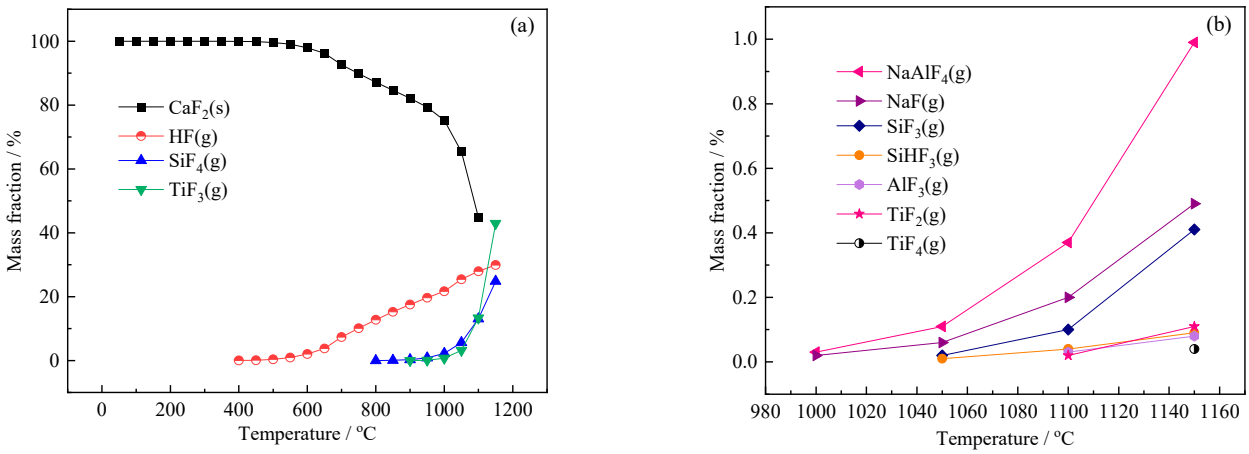

Figure 6. Distribution of the main fluorine products (**a**) and trace gaseous products (**b**) in different phases during the heating process.

Gaseous TiF_3 appeared at a calcination temperature of 900 °C, and its release increased with an increase in the calcination temperature. At 1150 °C, the mass fraction of TiF_3 was 42.94 wt%, and it was produced by the reaction of HF with titanium oxides [37] (Equation (22)). As shown in Figure 6b, when the calcination temperature exceeded 1000 °C, various trace fluorine-containing gases began to appear in the system, including $NaAlF_4$, NaF, SiF_3, $SiHF_3$, AlF_3, TiF_2, and TiF_4 (Figure 6b). It was hypothesized that these gaseous fluorides were formed due to a series of reactions between HF and metal oxides, or high-temperature solid products in raw materials. Therefore, the actual production process could reduce the production of large amounts of gaseous fluoride by appropriately lowering the temperature.

$$Ti_2O_3(s) + 6HF(g) \rightarrow 2TiF_3(g) + 3H_2O(g) \quad (22)$$

4. Environmental Impact Assessment and Management

In a previous study, the firing behavior of triaxial ceramsites and the presence of different phases were interpreted using FactSage [38]. Although this study analyzed the formation of the liquid phase and the crystallization of the mineral phase at different temperatures during ceramsites firing, it disregarded the generation of gaseous-phase substances at high temperatures, which might adversely affect the atmospheric environment. Therefore, this study predicted the possible gaseous pollutants generated when using carbide slag to prepare lightweight ceramsite, and proposed prevention and control methods to restrict the release of gaseous pollutants while exploring ways to render this process more environmentally friendly.

The migration and transformation of Al, C, H, S, and F, when using carbide slag for ceramsite preparation, were calculated and analyzed. The following conclusions were drawn: (1) Throughout the heating process (50–1150 °C), no Al-containing gas products were released, and they existed in the solid phase. (2) The C-containing gas-phase substance was mainly CO,

and its release increased with the increase in temperature. CO was formed via three routes: the reduction in C and O_2, the water–gas reaction of C and H_2O, and the high-temperature solid-state reaction between C and solid compounds (Fe_2O_3, CaS, and SiO_2). (3) The main H- and S-containing harmful gas was H_2S, which began to be released at 250 °C. H_2S was formed via two routes: the reduction in FeS and H_2, and the hydrolysis between H_2O, FeS, and CaS. (4) HF was the main H- and F-containing harmful gas, which began to be released at 400 °C. F-containing harmful gases began to appear at high temperatures (>1000 °C). Moreover, HF was produced via the hydrolysis of SiF_4, and SiF_4 was produced as a result of the high-temperature solid-state reaction between SiO_2 and CaF_2. TiF_3 was generated from the gas–solid reaction between HF and Ti_2O_3 at high temperatures.

Various gaseous pollutants were released throughout the calcination process during the preparation of lightweight ceramsite using carbide slag. At calcination temperatures above 1000 °C, the types of gaseous pollutants released increased significantly, such as CS_2, SiS, and various F-containing gases. Therefore, the calcination temperature was maintained below 1000 °C, which reduced the type and release of harmful gases. The main gaseous pollutants were H_2S, HF, and CO. CO is the basic raw material for the one-carbon chemical industry [39], while H_2S and HF are typical acidic gases [40]; CO can be recycled after the selective removal of H_2S and HF.

The goal of hazardous solid waste treatment is reduction and resource utilization [41]. The alkalinity of carbide slag is extremely high, with a pH value greater than 13 [42]. The alkaline slurry prepared from carbide slag can theoretically be effectively removed from the acid gas by acid-base neutralization [43]. Therefore, the removal of H_2S and HF used carbide slag slurry due to the inability of $Ca(OH)_2$ to react with CO.

On a laboratory scale, it was assumed that (1) no material loss occurred during the preparation of lightweight ceramic pellets; (2) H_2S and HF could be completely removed by the carbide slag slurry; and (3) no loss of CO occurred after passing through the carbide slag slurry.

The cost analysis for the preparation of SiO_2-Al_2O_3-CaO lightweight ceramsite is shown in Table 4. The cost of preparation of SiO_2-Al_2O_3-CaO lightweight ceramsite is ~91.42 $/ton, and the price of lightweight ceramsite in China is ~94.0 $/ton.

Table 4. Cost analysis for the preparation of SiO_2-Al_2O_3-CaO lightweight ceramsite.

Items	Price	Cost ($/ton)
Carbide slag (CaO)	~7.20 $/ton	~1.70
Natural sand (SiO_2)	~11.50 $/ton	~6.60
Bauxite (Al_2O_3)	~43.30 $/ton	~82.20
Electricity consumption	~0.14 $/(kW·h) [44]	~0.92 [44]
Total		~91.42

Combining the gas-phase equilibrium amounts of S, F, and C (Figure 1) and the distribution of S, F, and C products in different phases during the heating process, the amounts of H_2S, HF, and CO released during the preparation of one ton of lightweight ceramsite were calculated to be about 0.39 kg, 0.22 kg, and 1.99 kg, respectively. Based on the acid-base neutralization reactions, the carbide slag slurry consumption for removing 0.39 kg H_2S and 0.22 kg HF is ~1.21 kg. The price of carbide slag is ~7.20 $/ton, and the price of general waste liquid treatment is ~0.44 $/kg [45]. Thus, the treatment of waste gas produced by one ton of lightweight ceramsite cost ~0.54 $. Moreover, the current recovery price of CO is ~10.94 $/kg [46] and the potential value of CO generated from the production of one ton of lightweight ceramsite is ~21.77 $.

According to the aforementioned economic analysis, the profit margin of preparing SiO_2-Al_2O_3-CaO lightweight ceramsite is ~2.04 $/ton (the price of lightweight ceramsite minus expenses and exhaust treatment cost), and the potential value of the recoverable CO recovery is ~21.77 $/ton.

5. Conclusions

The preparation of lightweight ceramsite using carbide slag is essential to the resource utilization of carbide slag. In this study, the release and migration of elements during the lightweight ceramsite preparation were analyzed computationally for the first time, and treatment methods were proposed, aiming to promote the environmentally friendly process of lightweight ceramsite preparation using carbide slag.

This study found that various gaseous contaminants were released throughout the heating process (50–1150 °C) during the preparation of lightweight ceramsite, and maintaining the calcination temperature below 1000 °C prevented the formation of many trace gaseous contaminants. The main gaseous pollutants H_2S, HF, and CO needed treatment or recovery. The use of the lightweight ceramsite prepared using carbide slag could yield a profit of ~2.04 $/ton and the potential value of the recoverable CO was ~21.77 $/ton, which could simultaneously realize the reuse value of carbide slag, the resource value of CO, and the economic value of lightweight ceramsite.

Author Contributions: Conceptualization, M.J. and Y.H.; software, Z.W.; formal analysis, Q.J. and Y.W.; data curation, T.L. and C.L.; writing—original draft preparation, Q.J.; writing—review and editing, Q.J.; funding acquisition, M.J. and H.L. All authors have read and agreed to the published version of the manuscript.

Funding: This work was supported by the National Natural Science Foundation of China (No. 51768074) and Yunnan Agricultural Foundation Research Projects (202101BD070001-113) and Natural Science Foundation of Chongqing Municipal Science and Technology Commission (No. cstc2020jcyj-msxmX0833).

Data Availability Statement: The data used to support the findings of this study have not been made available because the experimental data involved in the paper are all obtained based on the authors' designed experiments and need to be kept confidential; they are still using the data for further research.

Acknowledgments: The authors wish to acknowledge and thank the reviewers and industry experts for their contributions towards the completion and publication of this article. The authors also wish to acknowledge and thank the support and contributions of colleagues, family, and friends.

Conflicts of Interest: The authors declare no conflict of interest.

References

1. Feng, Y.S.; Du, Y.J.; Zhou, A.; Zhang, M.; Li, J.S.; Zhou, S.J.; Xia, W.Y. Geoenvironmental properties of industrially contaminated site soil solidified/stabilized with a sustainable by-product-based binder. *Sci. Total Environ.* **2021**, *765*, 142778. [PubMed]
2. Sun, Z.; Chen, S.Y.; Ma, S.W.; Xiang, W.G.; Song, Q.B. Simulation of the calcium looping process (CLP) for hydrogen, carbon monoxide and acetylene poly-generation with CO_2 capture and COS reduction. *Appl. Energy* **2016**, *169*, 642–651. [CrossRef]
3. Wang, N.; Mao, M.; Mao, G.Y.; Yin, J.B.; He, R.X.; Zhou, H.C.; Li, N.; Liu, Q.S.; Zhi, K.D. Investigation on carbide slag catalytic effect of Mongolian bituminous coal steam gasification process. *Chemosphere* **2021**, *264*, 128500. [CrossRef] [PubMed]
4. Yang, H.; Cao, J.W.; Wang, Z.; Chen, H.H.; Gong, X.Z. Discovery of impurities existing state in carbide slag by chemical dissociation. *Int. J. Miner. Process.* **2014**, *130*, 66–73. [CrossRef]
5. Wang, Y.L.; Cui, S.P.; Wang, H.; Dong, S.J.; Yao, Y. Effects of preparation of cement raw meal with carbide slag on the environment and equipments. *Mater. Sci. Forum* **2014**, *787*, 123–127. [CrossRef]
6. Siyal, A.N.; Memon, S.Q.; Parveen, S.; Soomro, A.; Khaskheli, M.I.; Khuhawar, M.Y. Chemical recycling of expanded polystyrene waste: Synthesis of novel functional polystyrene-hydrazone surface for phenol removal. *J. Chem.* **2013**, *2013*, 842435. [CrossRef]
7. Maheswari, P.; Venilamani, N.; Madhavakrishnan, S.; Syed Shabudeen, P.S.; Venckatesh, R.; Pattabhi, S. Utilization of sago waste as an adsorbent for the removal of Cu(II) ion from aqueous solution. *J. Chem.* **2007**, *5*, 376839. [CrossRef]
8. Kizilkaya, B.; TekJnay, A.A. Utilization to remove Pb (II) ions from aqueous environments using waste fish bones by ion exchange. *J. Chem.* **2014**, *2014*, 739273.
9. Wang, Y.Q.; Li, Y.C.; Yuan, A.; Yuan, B.; Lei, X.R.; Ma, Q.; Han, J.; Wang, J.X.; Chen, J.Y. Preparation of calcium sulfate whiskers by carbide slag through hydrothermal method. *Cryst. Res. Technol.* **2014**, *49*, 800–807. [CrossRef]
10. Lv, S.Z.; Zhao, S.Y.; Liu, M.M.; Wu, P.P. Preparation of calcium carbonate by calcium carbide residue. *Adv. Mater. Res.* **2013**, *864*, 1963–1967. [CrossRef]
11. Altiner, M. Study of using calcium carbide slag to prepare calcium oxide briquettes by molding and calcination processes through Taguchi method. *Çukurova Univ. J. Fac. Eng. Archit.* **2008**, *31*, 179188.

12. Fan, J.J.; Cao, D.G.; Jing, Z.Z.; Zhang, Y.; Pu, L.; Jing, Y.N. Synthesis and microstructure analysis of autoclaved aerated concrete with carbide slag addition. *J. Wuhan Univ. Technol.-Mat. Sci. Edit.* **2014**, *5*, 1005–1010. [CrossRef]
13. Fang, D.X.; Huang, L.P.; Fang, Z.Y.; Zhang, Q.; Shen, Q.S.; Li, Y.M.; Xu, X.Y.; Ji, F.Y. Evaluation of porous calcium silicate hydrate derived from carbide slag for removing phosphate from wastewater. *Chem. Eng. J.* **2018**, *354*, 1–11. [CrossRef]
14. Jia, J.L.; Hu, L.; Zheng, J.X.; Zhai, Y.J.; Yao, P.; Zhao, S.W.; Shi, S.H.; Zhai, X.B.; Zhang, D.Y. Environmental toxicity analysis and reduction of ceramsite synthesis from industrial coal gasification coarse cinder waste. *Pol. J. Environ. Stud.* **2017**, *26*, 147–153. [CrossRef]
15. Sun, J.; Yang, M.; Zeng, L.; Wang, M.; He, S.; Cai, S.; Li, L.; Liu, X.; Zhang, H. Adsorption Performance on sediment nutrients by different proportions of zeolite and shale ceramsite (ZSC). *Pol. J. Environ. Stud.* **2020**, *29*, 2365–2372. [CrossRef]
16. Zhang, X.Y.; Li, X.; Han, Q.J.; Ju, K.; Wei, D.Y.; Sun, Y.Q.; Wan, Q. Effects of hydraulic retention time (HRT) and packing height on the performance of homemade ceramsite-soil constructed wetland for rural domestic wastewater treatment. *Pol. J. Environ. Stud.* **2021**, *30*, 4845–4854. [CrossRef]
17. Shi, Y.X.; Guo, W.C.; Jia, Y.L.; Xue, C.H.; Qiu, Y.X.; Zhao, Q.X.; Wang, D.L. Preparation of non-sintered lightweight aggregate ceramsite based on red mud-carbide slag-fly ash: Strength and curing method optimization. *J. Clean. Prod.* **2022**, *372*, 133788. [CrossRef]
18. Yao, S.W.; Zhang, W.B.; Xia, C.K. Process feasibility study for using quarry tailing for light granular. *Min. Eng.* **2018**, *16*, 60–63. (In Chinese)
19. Bale, C.W.; Chartrand, P.; Degterov, S.A.; Eriksson, G.; Hack, K.; Mahfoud, R.B.; Melançon, J.; Pelton, A.D.; Petersen, S. FactSage thermochemical software and databases, 2010–2016. *Calphad* **2016**, *54*, 35–53. [CrossRef]
20. Harvey, J.P.; Lebreux-Desilets, F.; Marchand, J. On the application of the Factsage thermochemical software and databases in materials science and pyrometallurgy. *Processes* **2020**, *8*, 1156. [CrossRef]
21. Junior, A.B.B.; Espinosa, D.C.R.; Tenório, J.A.S. The use of computational thermodynamic for yttrium recovery from rare earth elements-bearing residue. *J. Rare Earths* **2020**, *39*, 201–207. [CrossRef]
22. Fan, Y.Q.; Lyu, Q.G.; Zhu, Z.P.; Zhang, H.X. The impact of additives upon the slagging and fouling during Zhundong coal gasification. *J. Energy Inst.* **2020**, *93*, 1651–1665. [CrossRef]
23. Li, Y.; Li, F.H.; Ma, M.J.; Yu, B.; Zhao, C.Y.; Fang, Y.T. Prediction of ash flow temperature based on liquid phase mass fraction by FactSage. *J. Energy Inst.* **2020**, *93*, 2228–2231. [CrossRef]
24. Das, K.; Agrawal, A.; Reddy, A.S.; Ramna, R.V. Factsage studies to identify the optimum slag regime for blast furnace operation. *T. Indian. I. Metals.* **2021**, *74*, 419–428. [CrossRef]
25. Li, H.X.; Yoshihiko, N.; Dong, Z.B.; Zhang, M.X. Application of the FactSage to predict the ash melting behavior in reducing conditions. *Chin. J. Chem. Eng.* **2006**, *14*, 784–789. [CrossRef]
26. Tan, Y.D.; Wang, S.; Li, L.Z. Application of microwave heating for methane dry reforming catalyzed by activated carbon. *Chem. Eng. Process.* **2019**, *145*, 107662. [CrossRef]
27. Benchiheub, O.; Mechachti, S.; Serrai, S.; Khalifa, M.G. Elaboration of iron powder from mill scale. *J. Mater. Environ. Sci.* **2010**, *1*, 267–276.
28. Sun, W.Q.; Cai, J.J.; Zhang, D.W.; Guan, D.J. Advanced low-carbon technologies for steel manufacturing process. *Appl. Mech. Mater.* **2010**, *44–47*, 8–12. [CrossRef]
29. Chen, C.; Li, H.J.; Bai, Y.; Feng, F.X.; Tian, L.; Yang, Y.; Liu, Y.; Guo, Q. Effect of sulfidation temperature on component transformation and catalytic performance of direct coal liquefaction catalyst. *J. Fuel Chem. Technol.* **2022**, *50*, 54–62. [CrossRef]
30. Yang, S.T.; Zhou, M.; Jiang, T.; Guan, S.F.; Zhang, W.J.; Xue, X.X. Application of a water cooling treatment and its effect on coal-based reduction of high-chromium vanadium and titanium iron ore. *Int. J. Min. Met. Mater.* **2016**, *23*, 1353–1359. [CrossRef]
31. Jiang, M.; Liu, H.P.; Fan, X.D.; Wang, Z.H. Predicting gaseous pollution of sintered brick preparation from yellow phosphorus slag. *Pol. J. Environ. Stud.* **2019**, *28*, 1719–1725. [CrossRef]
32. Dowaki, K.; Kuroda, S.; Saruya, H. A LCA on the H_2S and HCl removal procedures using in HAS-Clays. *J. Jpn. Inst. Energy* **2018**, *97*, 160–170. [CrossRef]
33. Fetisov, E.O.; Shah, M.S.; Knight, C.; Tsapatsis, M.; Siepmann, J.I. Understanding the reactive adsorption of H_2S and CO_2 in sodium-exchanged zeolites. *ChemPhysChem* **2017**, *19*, 512–518. [CrossRef]
34. Zhang, T.L.; Yang, C.; Feng, X.K.; Wang, Z.Q.; Wang, R.; Liu, Q.L.; Zhang, P.; Wen, L. Theoretical study on the atmospheric reaction of HS with HO_2: Mechanism and rate constants of the major channel. *Acta Phys-Chim Sin.* **2016**, *32*, 701–710. [CrossRef]
35. Li, P.; Li, H.; Jie, W. Stabilization of lanthanum sulfides with different dopants. *J. Wuhan Univ. Technol.-Mat. Sci. Edit.* **2012**, *27*, 529–533. [CrossRef]
36. Chang, H.Q.; Wang, H.Y.; Zhang, G.H.; Chou, K.C. Controllable syntheses of Mo_5Si_3 and Mo_3Si by silicothermic reduction of MoS_2 in the presence of lime. *Ceram. Int.* **2022**, *48*, 7815–7826. [CrossRef]
37. Nakagawa, M.; Matsuya, S.; Shiraishi, T.; Ohta, M. Effect of fluoride concentration and pH on corrosion behavior of titanium for dental use. *J. Dent. Res.* **1999**, *78*, 1568–1572. [CrossRef]
38. Baccarin, L.I.P.; Bielefeldt, W.V.; Bragança, S.R. Evaluation of thermodynamic simulation (FactSage) for the interpretation of the presence of phases and the firing behavior of triaxial ceramics. *Ceram. Int.* **2021**, *47*, 21522–21529. [CrossRef]
39. Du, C.; Lu, P.; Tsubaki, N. Efficient and new production methods of chemicals and liquid fuels by carbon monoxide hydrogenation. *ACS Omega* **2020**, *5*, 49–56. [CrossRef]
40. Hansell, A.; Oppenheimer, C. Health hazards from volcanic gases: A systematic literature review. *Arch. Environ. Health* **2004**, *59*, 628–639. [CrossRef]

41. Guo, W.; Xi, B.; Huang, C.; Li, J.; Wu, W. Solid waste management in China: Policy and driving factors in 2004–2019. *Resour. Conserv. Recycl.* **2021**, *173*, 105727. [CrossRef]
42. Yang, J.; Ma, L.P.; Liu, H.P.; Wei, L.; Keomounlath, B.; Dai, Q.X. Thermodynamics and kinetics analysis of Ca-looping for CO_2 capture: Application of carbide slag. *Fuel* **2019**, *242*, 1–11. [CrossRef]
43. Wang, H.; Xu, W.; Sharif, M.; Cheng, G.; Zhang, Z. Resource utilization of solid waste carbide slag: A brief review of application technologies in various scenes. *Waste Dispos. Sustain. Energy* **2022**, *4*, 1–16. [CrossRef]
44. Zhao, L.N.; Hu, M.; Muslim, H.; Hou, T.Y.; Bian, B.; Yang, Z.; Yang, W.B.; Zhang, L.M. Co-utilization of lake sediment and blue-green algae for porous lightweight aggregate (ceramsite) production. *Chemosphere* **2022**, *287*, 132145. [CrossRef]
45. Parrish, C.F.; Barile, R.G.; Gamble, P.H. A new process and equipment for waste minimization: Conversion of No(X) scrubber liquor to fertilizer. In Proceedings of the Joint Army, Navy, NASA, Air Force (JANNAF) Conference, Tampa, FL, USA, 4–8 December 1995; p. 19960011436. Available online: https://ntrs.nasa.gov/citations/19960011436 (accessed on 6 September 2013).
46. Shae, S.Y.; Lee, S.Y.; Han, S.G.; Kim, H.; Ko, J.; Park, S.; Joo, O.-S.; Kim, D.; Kang, Y.; Lee, U.; et al. A perspective on practical solar to carbon monoxide production devices with economic evaluation. *Sustain. Energy Fuels* **2020**, *4*, 199.